

1 Supplement of  
2 **Measurement report: Long emission-wavelength chromophores dominate the light absorption**  
3 **of brown carbon in Aerosols over Bangkok: impact from biomass burning**

4 Jiao Tang et al.

5  
6 **Correspondence:** Guangcai Zhong ([gczhong@gig.ac.cn](mailto:gczhong@gig.ac.cn))

7  
8 **Content of this file**

9 Text S1 to S4

10 Table S1 to S5

11 Figure S1 to S16

12

### Text S1. Analysis of carbon content

The concentration of WSOC was quantified using a TOC analyzer (Vario TOC cube; Elementar). All WSOC concentrations were blank corrected. The concentration of OC in MSOC was calculated as the difference between the OC and WSOC concentrations. The calculation assumed that all water-insoluble organic carbon in the aerosols can be extracted with methanol (Cheng et al., 2016). Chen et al. (2019) reported that only a small amount of organic carbon (OC, 6%) were extracted with DCM after water and methanol extraction, thus we assumed that methanol can extract the majority of the extractable OC in the aerosols.

### Text S2. Analysis of UV-visible Absorption spectra

Absorption Ångström exponent (AAE) represents the wavelength dependence of absorption is calculated according to following formula (Fan et al., 2018):

$$A = K \cdot \lambda^{-AAE} \quad (1)$$

Here, A is the measured absorbance, and K is constant. 330 nm to 400 nm is selected for fitting AAE value.

Light absorption coefficient ( $Abs_\lambda$ ,  $Mm^{-1}$ ) can be calculated using the following formula (Yan et al., 2015):

$$Abs_\lambda = \frac{(A_\lambda - A_{700}) \times V_1 \times a \times \ln(10)}{Va \times a_1 \times l} \quad (2)$$

Here,  $A_\lambda$  is the value of light absorption at the given wavelength given by the spectrophotometer;  $V_1$  and  $a_1$  is the volume of ultra-pure deionized water or methanol for extraction and area of the extracted filter;  $Va$  is the volume of sampling air;  $l$  is the optical path length.

Mass absorption efficiency (MAE,  $m^2 g^{-1} C$ ) can be obtained as follows (Cheng et al., 2011):

$$MAE_\lambda = \frac{Abs_\lambda}{C_i} \quad (3)$$

Here,  $C_i$  ( $\mu g C/m^3$ ) is the concentration of WSOC and MSOC after conversion to the atmosphere. Moreover, the pH was measured for all samples within the range of 5–7, generally thought it didn't affect the absorbance according to prior study (Chen et al., 2016a).

To understand the importance of BrC in radiative forcing, its relative light absorption contribution to total aerosols was estimated by assuming that BrC and BC externally mixed in aerosols (Cheng et al., 2011). The relative contribution of each aerosol extract to the total light-absorption by the organics and EC was assessed. The total light-absorptions of the different aerosol extracts and EC were calculated from the MAEs of the organics and EC and their atmospheric concentrations using the following equation:

$$Abs_{\lambda, total} = \sum_i MAE_{\lambda, i} \cdot C_i + MAE_{\lambda, EC} \cdot C_{EC} \quad (4)$$

where  $C_i$  is the concentration of the organics in extract  $i$  (i.e., WSOC, and MSOC) when they were in the atmosphere ( $\mu\text{g C m}^{-3}$ ). The concentrations of  $C_{EC}$  were measured by thermal-optical (or thermal) method is typically used as BC (Cheng et al., 2011). The MAE of EC in the range of 250–700 were calculated, and MAE in the aerosols is expressed as a function of AAE (Chen et al., 2016a; Lee et al., 2014; Andreae and Gelencsér, 2006):

$$MAE_{\lambda} = a \cdot \lambda^{-AAE} \quad (5)$$

where  $a$  is a constant that is related to the light-absorptivity; the AAE values and MAE of EC at 550 nm assumed to be 1 and  $7.5 \text{ m}^2 \text{ g}^{-1}$ , respectively (Bond and Bergstrom, 2006). And the variability of MAE and AAE is considered as 6.3–8.7 and 0.8–1.4, respectively (Liu et al., 2018a; Chen et al., 2016a; Bond and Bergstrom, 2006).

Figure S12 showed the relative contributions of each of the aerosol extracts to the total light absorption of the aerosols. In the low-UV region (250–300 nm), the light absorption of WSOC and MSOC fractions was higher than that of BC. At 250 nm, the light absorption of extracted BrC is as large as  $35 \text{ Mm}^{-1}$ , which is 1.5 times higher than the BC, and decreased to  $19 \text{ Mm}^{-1}$  at 300 nm with comparable values to the light absorption by BC. Although the significant UV absorption at wavelengths below 300 nm may not be important for the transfer of total solar radiation in the troposphere, the presence of light-absorbing organic aerosols may cause a reduction in UV photolysis and the near-surface ozone mixing ratios (Barnard et al., 2008). By contrast, the total light absorption by WSOC and MSOC is only  $7.3 \text{ Mm}^{-1}$  at 365 nm, accounting for an average of 28% of total light absorption. Xie et al. (2019a) observed higher contributions of BrC to the total absorption at 370 nm at ground level and 260m, on average accounting for 46% and 48%, respectively. In the visible region (400–600 nm), the extracted BrC contributed from an average of 21% of total absorption at 400 nm to 8.0% at 500 nm to below 4.0% at 600 nm and decreased continuously toward longer wavelengths. Hoffer et al. (2006) estimated that the contribution of HULIS to light absorption was only a few percent in Amazonia biomass burning aerosols at 532 nm and 35%–50% at 300 nm. Wu et al. (2019) reported water-soluble BrC contributed 25.3% of total light absorption at 300 nm by aerosols from Godavari, which was lower than our result ( $35\% \pm 11\%$ ). However, it should be noted that the measured absorption of BrC in extracts may be underestimated by a factor of about 2 than that in ambient conditions due to incomplete extraction of OC by solvents and size-dependent absorption properties of organic aerosol (Shetty et al., 2019; Liu et al., 2013). Although a large amount of BrC were extracted by ultra-pure deionized water, and then methanol, there were non- and low-polar compounds that could not be extracted by the two solvents, such as aliphatic hydrocarbon structures, phthalate esters, and some polycyclic

aromatic hydrocarbons (Chen et al., 2017b). Thus, the actual absorption contribution of BrC in ambient conditions may be higher than the estimate of this study.

Generally, the AAE of BC particles is widely accepted to be 1.0, and this value was applied to calculate the MAE of BC in this study. However, a previous study reported BC AAE is not 1.0, even when BC is assumed to have small sizes and a wavelength-independent refractive index (Liu et al., 2018a), and vary from 0.8 to 1.4. The  $MAE_{550, BC}$  is  $7.5 \text{ m}^2 \text{ g}^{-1}$  at 550 nm for uncoated particles referring to previous study and the standard deviation is  $1.5 \text{ m}^2 \text{ g}^{-1}$  (Bond and Bergstrom, 2006), which is used to calculate the MAE of BC at a different wavelength. Thus, the uncertainty of light absorption of BC in the studied wavelength of 250–700 nm was calculated from 13% to 44%.

### Text S3. Quantifying spectral similarity

The Tucker congruence coefficient (TCC) is used for identifying similar spectra (Murphy et al., 2014), which increase its sensitivity to shape differences and peak shifts (Wünsch et al., 2019).

$$TCC(x, y) = \frac{\sum x y}{\sqrt{\sum x^2 \sum y^2}} \quad (6)$$

Where  $x$  and  $y$  are loading of two factors with identical x-axis-scale. TCCs are calculated for emission and excitation spectra ( $TCC_{ex}$  and  $TCC_{em}$ ) to form the overall  $TCC_{em \times ex}$ . TCC which is higher than 0.95 means high similarity.

### Text S4. Quality control

In this study, the relative standard deviation of WSOC concentration of parallel experiments of ambient particle samples based on method and instrument were 2.8% and 0.3%–4.6%. The error of WSOC concentration in five blank samples was 8.3%. The error of OC with value of 5.5% is presented in previous study (Wang et al., 2020). Thus, the calculated error of MSOC concentration is 10%. We corrected the procedural blank concentrations of WSOC concentration.

The value of absorbance of WSOC for field blank samples at 365 nm was 0.00063, and that of MSOC was lower than method detection limit (MDL). MDL was calculated based on the average of three blank samples at 365 nm adding the three times standard deviation, with values of 0.00057 and 0.00014 for WSOC and MSOC, respectively. The standard deviation of three-group parallel experiments of absorbance at 250–700nm were  $0.00015 \pm 0.00013$ ,  $0.0095 \pm 0.0091$ , and  $0.00002 \pm 0.00002$ . Further, no obvious peak was found in the fluorescence spectrum of field blank samples. The fluorescence spectrum of samples was measured with their absorbance lower than 1.

107 **Table S1** The average meteorological data (mean±S. D.) in different seasons over Bangkok in Thailand from January  
 108 2016 to January 2017.

	Month	Temperature (° F)	Humidity (%)	Wind Speed (mph)	Pressure
Pre-hot season	Jan.–Feb.	82±5.0	67±11	6.2±1.9	30±0.067
Hot season	Mar.–May.	89±2.5	68±7.3	8.8±1.4	30±0.12
Monsoon	Jan, and Oct.	84±2.2	81±8.2	6.2±1.6	30±0.059
Cool season	Nov. –Jan.	83±2.4	70±8.1	6.0±1.4	30±0.058

109

110 **Table S2** Fluorescent components identified by parallel factor analysis (PARAFAC) in water-soluble organic carbon  
 111 (WSOC) and methanol-soluble organic carbon (MSOC) in aerosol samples over Bangkok, Thailand (85-model), and  
 112 their Tucker congruence coefficient (TCC) values with components of 145-model containing ambient aerosol  
 113 samples and source samples.

Components (85-model)	Excitation maxima (nm)	Emission maxima (nm)	Assignment according to previous studies	145-model components	TCC values	References
P1	290	356	Protein-like fluorophore	145M-P3	0.94	(Qin et al., 2018;Fan et al., 2016)
P2	<250/308	415	Humic-like substances	145M-P1	0.97	(Chen et al., 2017a;Stedmon and Markager, 2005;Wu et al., 2019)
P3	254/356	443	The fluorescence of aqueous reactions of hydroxyacetone with glycine, or humic-like substances	145M-P6	0.90	(Gao and Zhang, 2018;Chen et al., 2003)
P4	257/386	513	Humic-like substances	145M-P5	0.96	(Chen et al., 2017a;Stedmon and Markager, 2005;Wu et al., 2019)
P5	<250	383		145M-P4	0.97	

P6	<250/332	392	N-containing SOA species, pyridoxine, or humic-like substances	145M-P7	0.97	(Babar et al., 2017; Pohlker et al., 2012; Chen et al., 2003)
P7	278	310	Tyrosine-like fluorophore, non-N-containing species	145M-P8	0.90	(Chen et al., 2016b; Zhou et al., 2019)
C1	<250	434	Fulvic acid-like substances	145M-C1	0.99	(Chen et al., 2003)
C2	<250	383	Fulvic acid-like substances	145M-C3	0.99	(Chen et al., 2003)
C3	287	351		145M-C2	0.97	
C4	260	513		145M-C4	0.97	
C5	<250	360		145M-C5	0.93	
C6	275	306	Tyrosine-like fluorophore	145M-C7	0.98	(Stedmon and Markager, 2005)

114

115 **Table S3** Comparisons of light absorption of aerosol samples from Bangkok with the other studies.

Samples	Sites	Fraction	AAE	MAE <sub>365</sub> (m <sup>2</sup> g <sup>-1</sup> C)	References
TSP	Thailand	Water-soluble BrC	5.1±0.68	0.83±0.25	This study
		Methanol-soluble BrC	5.2±0.94	0.26±0.12	
PM <sub>10</sub>	Nepal	Water-soluble BrC		0.59 ± 0.16 in the monsoon season 1.05 ± 0.21 in the pre-monsoon season	(Wu et al., 2019)
PM <sub>2.5</sub>	Beijing	Water-soluble BrC	5.30 ± 0.44 in winter 5.83 ± 0.51 in summer	1.54 ± 0.16 in winter 0.73 ± 0.15 in summer	(Yan et al., 2015)
TSP	Guangzhou	Water-soluble BrC	5.33±0.71	0.81±0.16	(Liu et al., 2018b)
PM <sub>2.5</sub>	Beijing	Water-soluble BrC		1.79±0.24 in winter 0.71±0.20 in summer	(Cheng et al., 2011)

PM <sub>2.5</sub>		Water-soluble BrC		0.76	(Chen et al., 2018)
PM <sub>2.5</sub>	Southeastern US	Water-soluble BrC		0.29±0.13	(Xie et al., 2019b)
PM <sub>2.5</sub>	South Asia	Water-soluble BrC	4.00–4.44 in Deihi 5.11–6.68 in BCOB 6.63–7.13 in MCOH	2.24–2.49 in Deihi 1.35–1.45 in BCOB 0.31–0.52 in MCOH	(Dasari et al., 2019)
PM <sub>2.5</sub>	Beijing	Water-soluble BrC	5.27 ± 0.81	1.05 ± 0.32	(Mo et al., 2018)
PM <sub>2.5</sub>	Simulated biomass burning	Water-soluble BrC	7.40–9.03	0.86–1.23	(Fan et al., 2018)
PM <sub>2.5</sub>	Simulated biomass burning	Water-soluble BrC		0.76–1.44	(Park and Yu, 2016)
	Simulated biomass burning	Water-soluble BrC	7.1±1.6	1.6 ± 0.55	
	Simulated anthracite combustion	Water-soluble BrC		1.3 ± 0.34	
	Vehicle emission	Water-soluble BrC		0.71 ± 0.30	(Tang et al., 2020b; Tang
TSP	Simulated biomass burning	Methanol-soluble BrC		2.3 ± 1.1	et al., 2020a)
	Simulated anthracite combustion	Methanol-soluble BrC		0.88 ± 0.74	
	Vehicle emission	Methanol-soluble BrC		0.26 ± 0.09	

116

117 **Table S4** Summary of multiple linear regression results between light absorption at 365 nm (Abs<sub>365</sub>, Mm<sup>-1</sup>) of water-  
118 soluble BrC and its individual chromophore identified by parallel factor analysis in aerosol samples over Bangkok.

Model	Unstandardized coefficients		Standardized coefficients	t-STAT	p-Value
	B	Standard error	Beta		
<b>Regression 1:</b> n=85, R <sup>2</sup> = 0.994, Adjust R <sup>2</sup> = 0.994, error=0.38295					
P4 component	0.923	0.008	0.997	117.85	0.000
<b>Regression 2:</b> n=85, R <sup>2</sup> = 0.994, Adjust R <sup>2</sup> = 0.994, error=0.37123					
P4 component	0.898	0.013	0.97	71.382	0.000
P2 component	0.02	0.008	0.034	2.515	0.014
<b>Regression 3:</b> n=85, R <sup>2</sup> = 0.995, Adjust R <sup>2</sup> = 0.995, error=0.36385					

P4 component	0.765	0.065	0.826	11.767	0
P2 component	0.051	0.017	0.088	3.033	0.003
P7 component	0.091	0.044	0.107	2.088	0.04
<b>Regression 4:</b> n=85, $R^2 = 0.995$ , Adjust $R^2 = 0.995$ , error=0.35652					
P4 component	0.979	0.121	1.057	8.104	0
P2 component	0.041	0.017	0.071	2.399	0.019
P7 component	0.14	0.049	0.165	2.875	0.005
P3 component	-0.164	0.079	-0.275	-2.089	0.04

**Note:** Pre multiple linear regression (MLR), curve estimation was conducted to estimate the possible correlations between the dependent and independent variables. Statistical parameters were computed as the goodness-of-fit indicators including adjusted  $R^2$ , t-STAT (ratio of coefficient to standard error),  $p$ -value (target < 0.05). For the independent variables with significant correlations with the dependent variable ( $p$ -value < 0.05), or with positive contributions to the independence, Abs<sub>365</sub>, they will be retained in the statistical model as the efficiency factors to the Abs<sub>365</sub>. To simplify the model, non-significant independences, as well as constant, were gradually removed.

**Table S5** Summary of multiple linear regression results between light absorption at 365 nm (Abs<sub>365</sub>, Mm<sup>-1</sup>) of methanol-soluble BrC and its individual chromophore identified by parallel factor analysis in aerosol samples over Bangkok.

Model	Unstandardized coefficients		Standardized coefficients	t-STAT	p-Value
	B	Standard error	Beta		
<b>Regression 1:</b> n=85, R <sup>2</sup> = 0.945, Adjust R <sup>2</sup> = 0.944, error=0.33609					
C4 component	0.238	0.006	0.972	37.738	0.000
<b>Regression 2:</b> n=85, R <sup>2</sup> = 0.957, Adjust R <sup>2</sup> = 0.956, error=0.29861					
C4 component	0.489	0.052	1.998	9.317	0.000
C1 component	-0.119	0.025	-1.032	-4.811	0.000



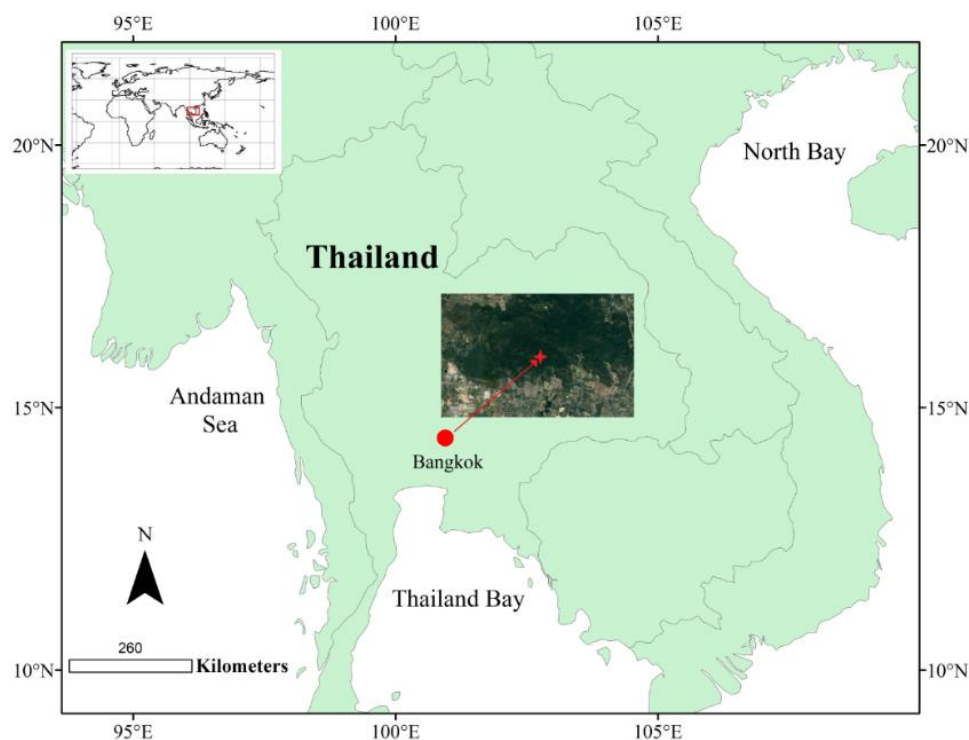


**Figure S1.** Location of sampling site at the faculty of the environment of Kasetsart University in Bangkok, Thailand. The basemap was drawn by ArcGIS software (ESRI Inc. California, USA). The satellite image at the center was derived from Google Maps (Image © Google Maps 2019).

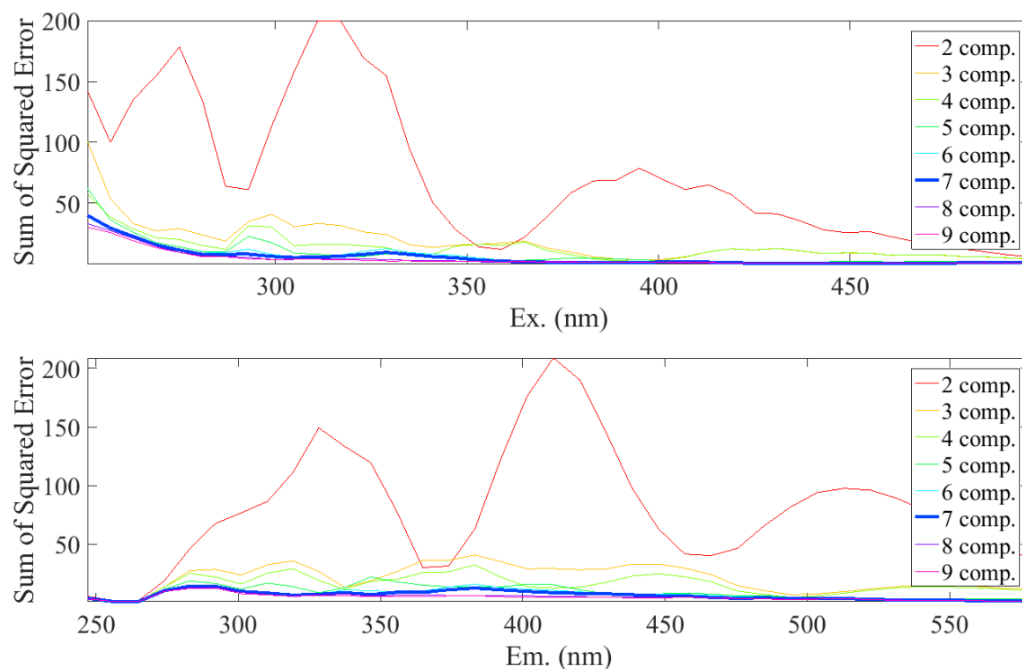
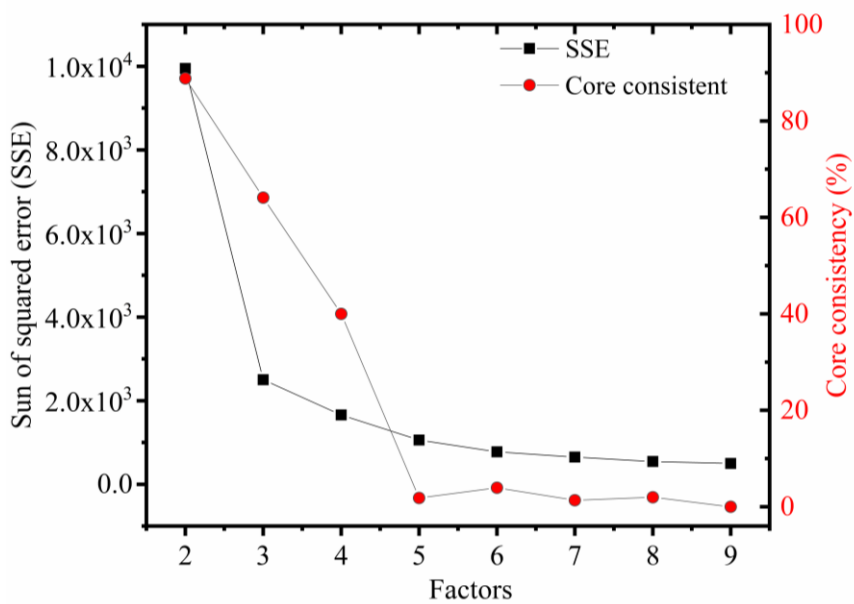


**Figure S2.** Sum of squared error of excitation and emission wavelength for 2–9 PARAFAC model in the WSOC in aerosol samples from Bangkok (n=85).

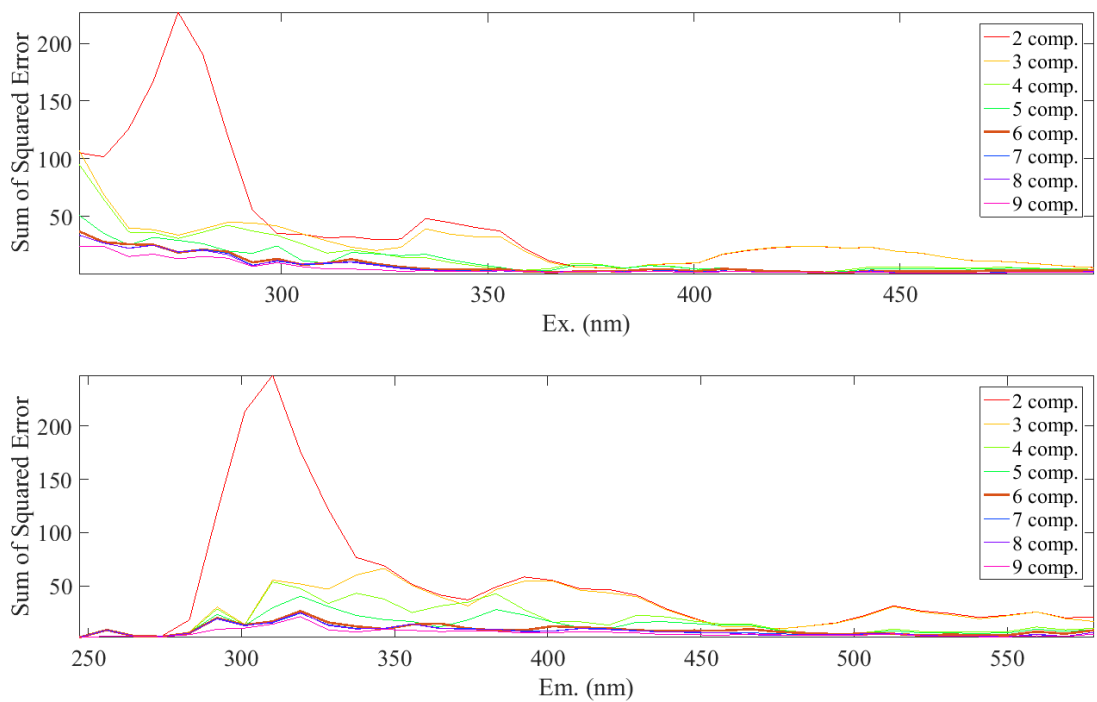
139



140

141 **Figure S3.** Sum of squared error (SSE) and core consistency of each PARAFAC model in the WSOC in aerosol  
142 samples from Bangkok (n=85).

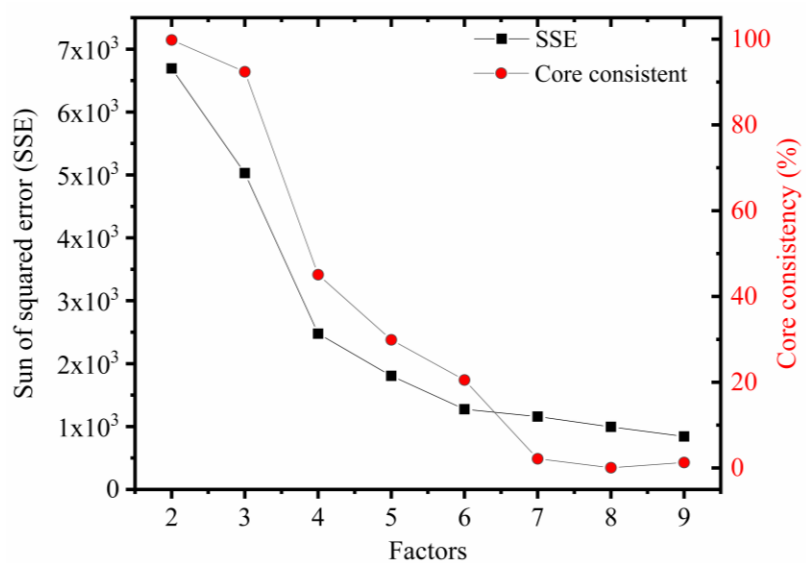
143



144

145 **Figure S4.** Sum of squared error of excitation and emission wavelength for 2–9 PARAFAC model in the MSOC  
146 fraction in aerosol samples from Bangkok (n=85).

147



148

149 **Figure S5.** Sum of squared error (SSE) and core consistency of each PARAFAC model in the MSOC in aerosol  
 150 samples from Bangkok (n=85).

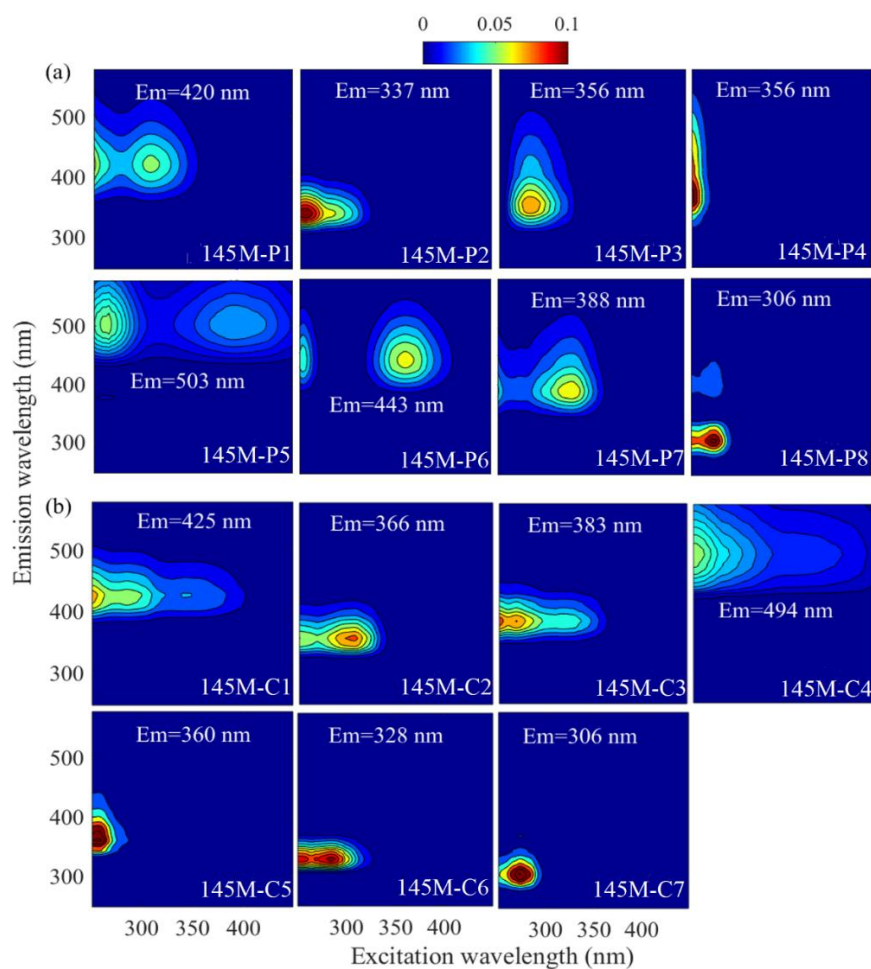


**Figure S6.** The eight fluorescent components of the WSOC (a, 145-model, 145M-P1–8) and seven fluorescent components of the MSOC (b, 145-model, 145M-C1–8), respectively, identified by the PARAFAC method in aerosol samples from Bangkok, Thailand, and source samples (n=145).

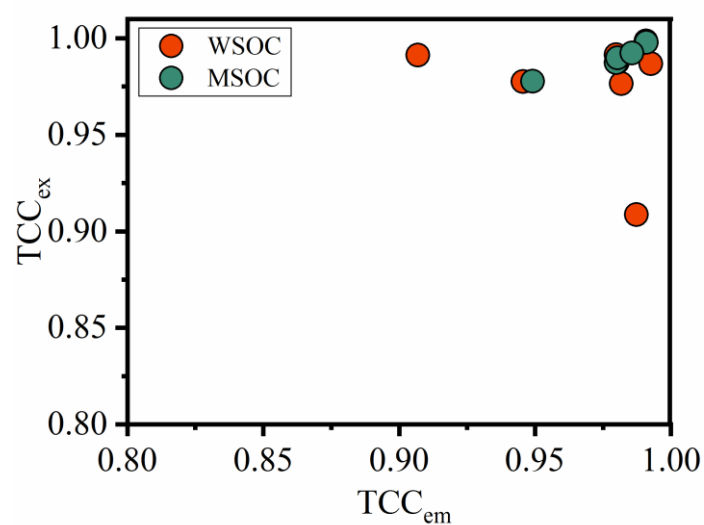


**Figure S7.** Evaluation of fluorescence emission and excitation spectrum similarity of 85-model with 145-model by Tucker congruence coefficient (TCC).

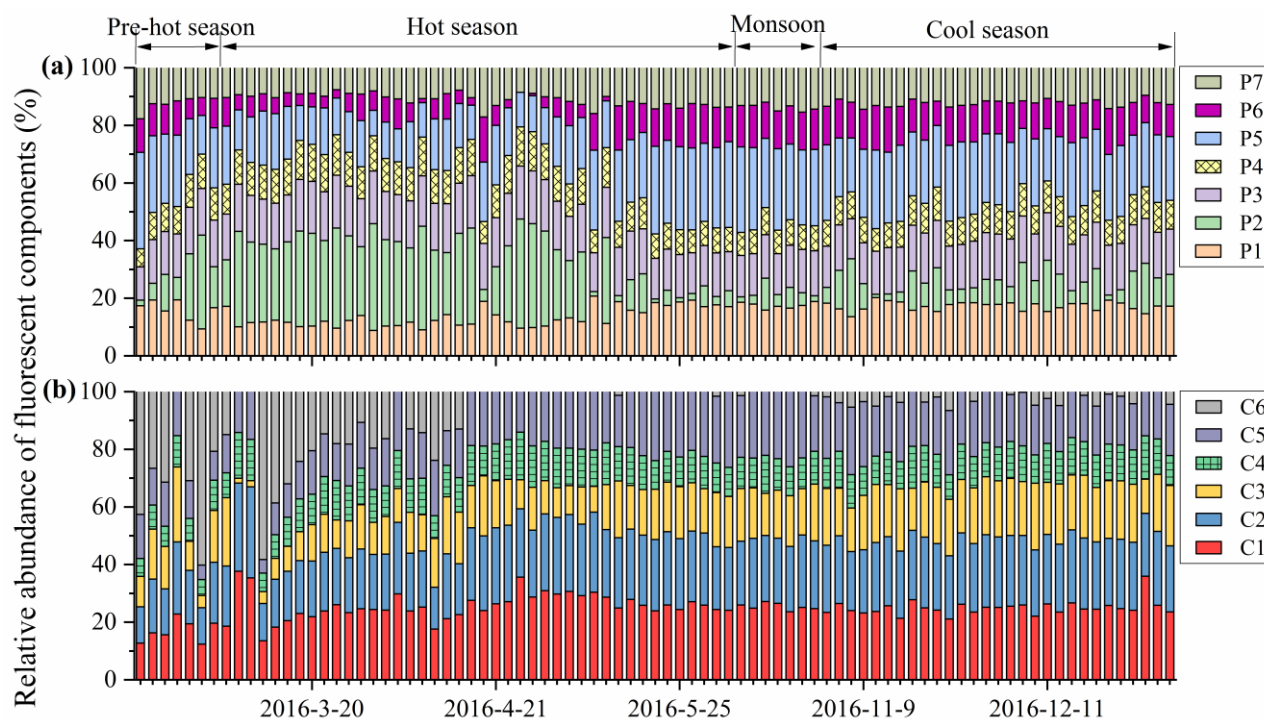


**Figure S8.** Relative abundances of the PARAFAC-derived components of WSOC (a, P1–7) and MSOC (b, C1–6) of aerosol samples over Bangkok in Thailand (85-model). Pre-hot season is from January 18 to February 29, 2016; hot season is from March 2 to May 31, 2016; monsoon is from June 2 to October 30, 2016; cool season is from November 1, 2016 to January 28, 2017.

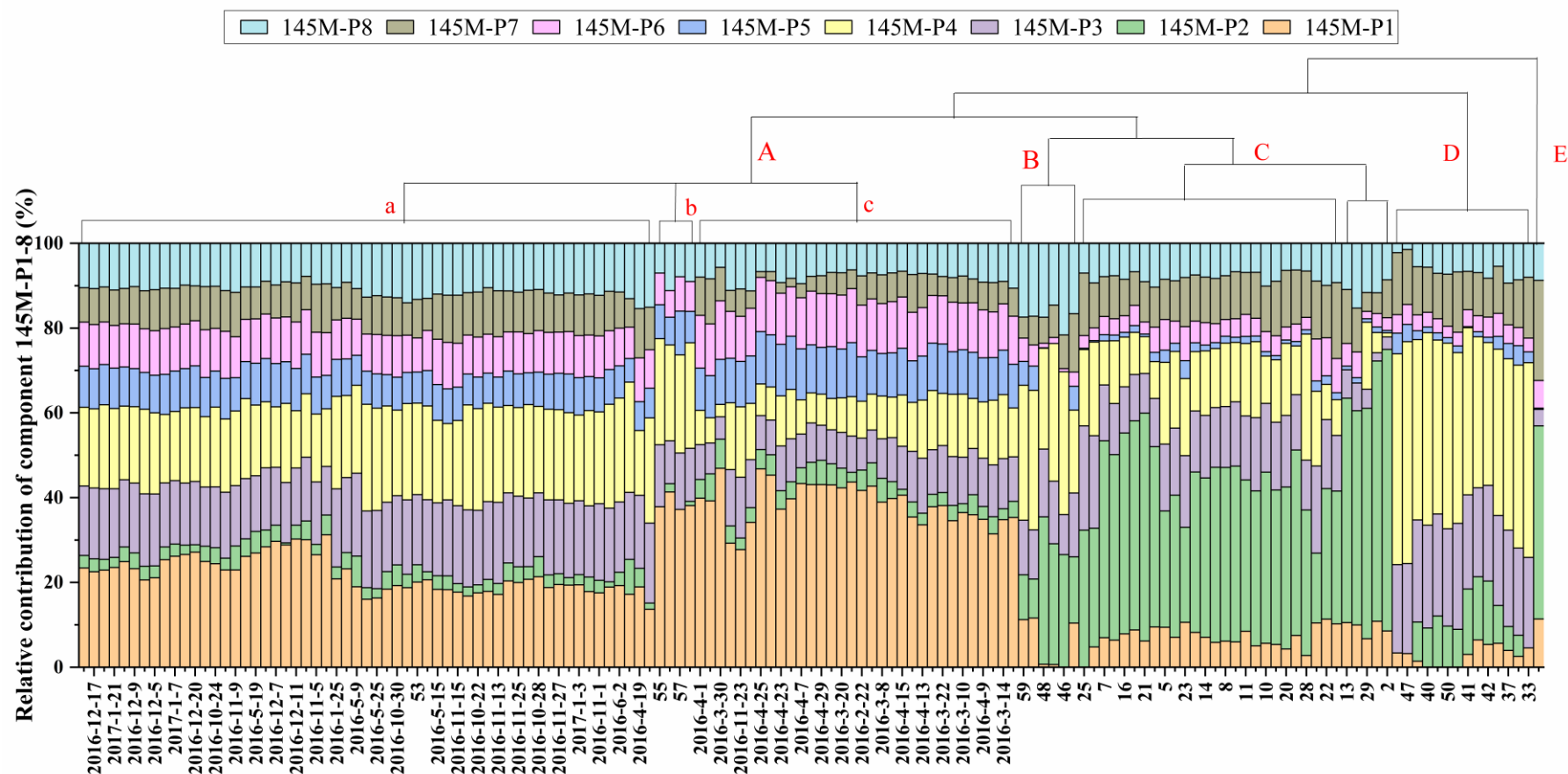


**Figure S9.** Hierarchical cluster analysis based on the relative contributions of PARAFAC-derived components (145-model, 145M-P1–8) in the WSOC. The sample IDs correspond to different types of aerosols as follows: ID 1–33: aerosol samples from simulated biomass burning; ID 34–50: aerosol samples from simulated coal combustion; ID 51–58: aerosol samples collected in the tunnel; ID 59–60: aerosol samples from vehicle exhaust.

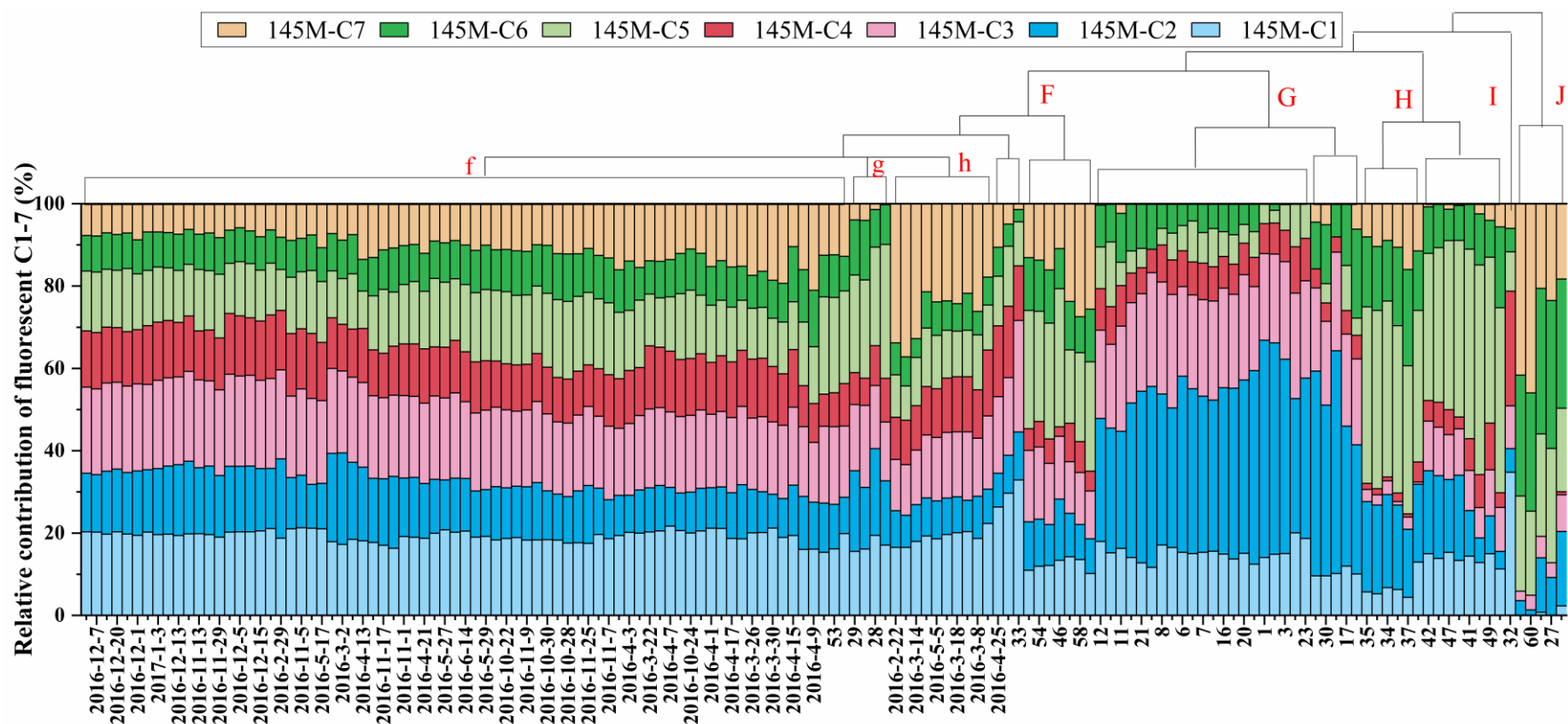


**Figure S10.** Hierarchical cluster analysis based on the relative contributions of PARAFAC-derived components (145-model, 145M-C1–7) in the MSOC. The sample IDs correspond to different types of aerosols as follows: ID 1–33: aerosol samples from simulated biomass burning; ID 34–50: aerosol samples from simulated coal combustion; ID 51–58: aerosol samples collected in the tunnel; ID 59–60: aerosol samples from vehicle exhaust.

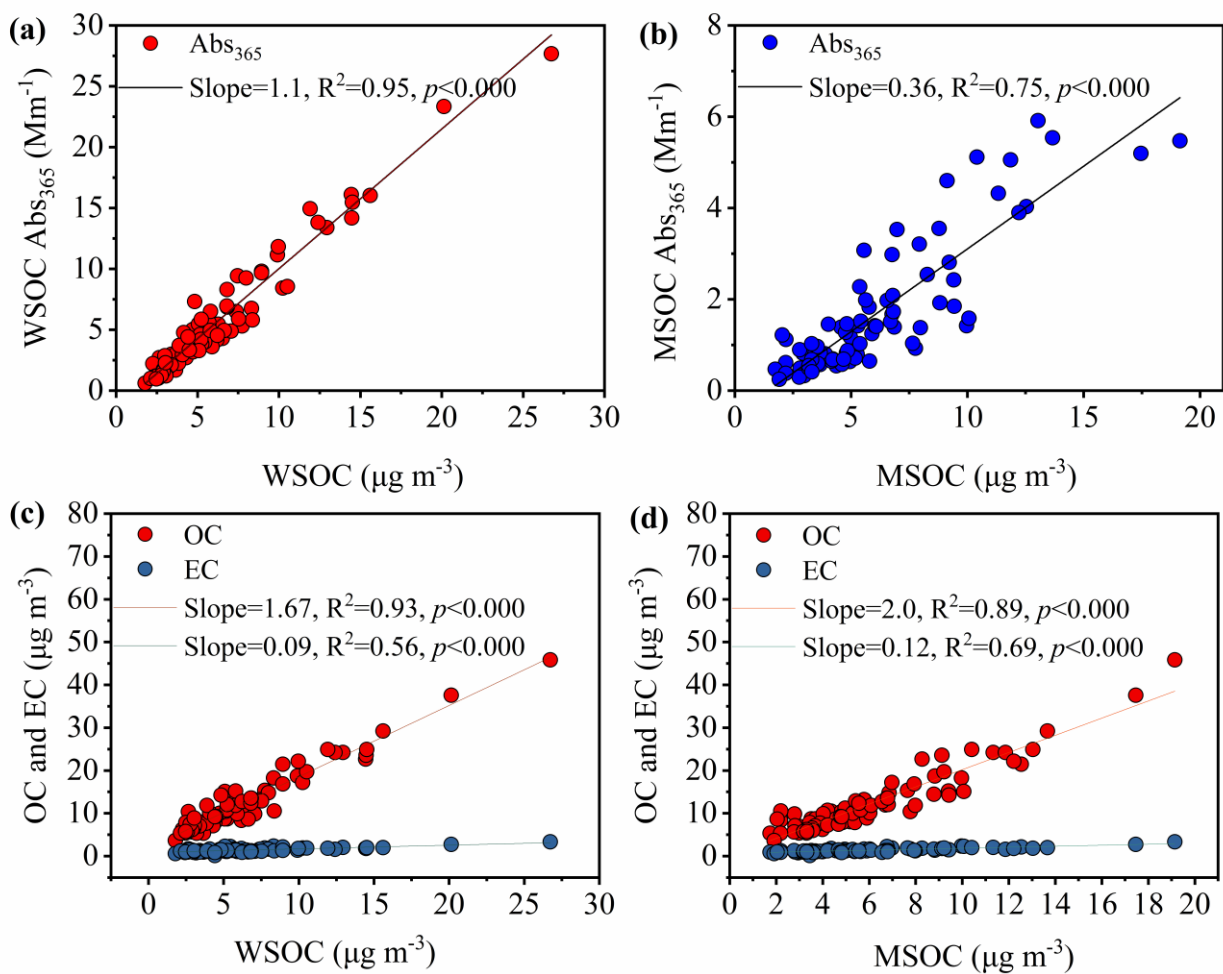


**Figure S11.** Scatter plots of  $Abs_{365}\ (Mm^{-1})$  of water-soluble BrC versus  $WSOC\ (\mu g\ C\ m^{-3})$  (a) and  $Abs_{365}\ (Mm^{-1})$  of methanol-soluble BrC versus  $MSOC\ (\mu g\ C\ m^{-3})$  (b), and  $WSOC$  versus  $OC$  and  $EC$  (c) and  $MSOC$  versus  $OC$  and  $EC$  (d) in aerosol samples from Bangkok, Thailand, respectively. Where the slope (a and b) is defined as the  $WSOC$  or  $MSOC$  mass absorption efficiency (MAE, solvent extract absorption at 365 nm per  $WSOC$  or  $MSOC$  mass  $m^2\ g^{-1}$  C).



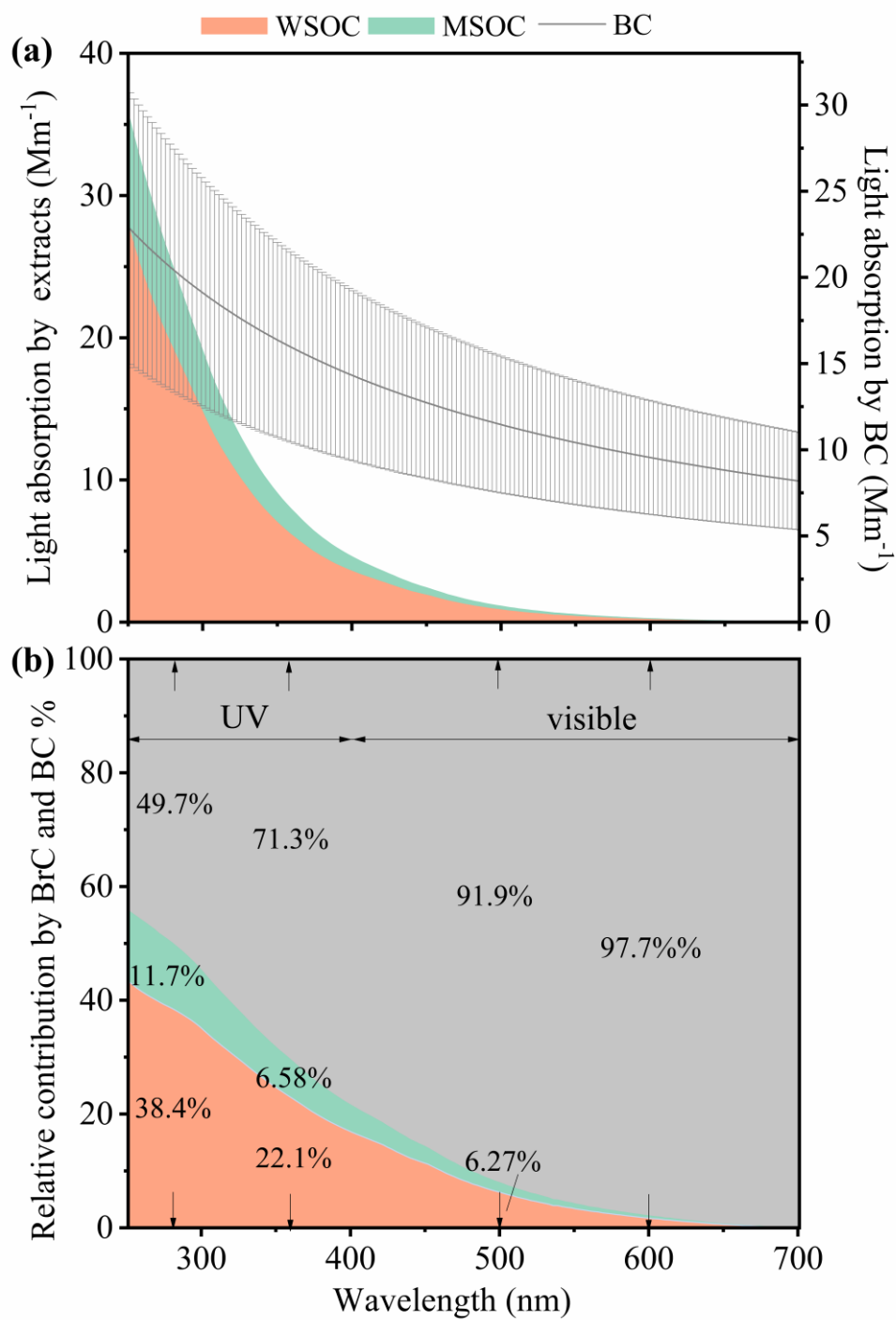
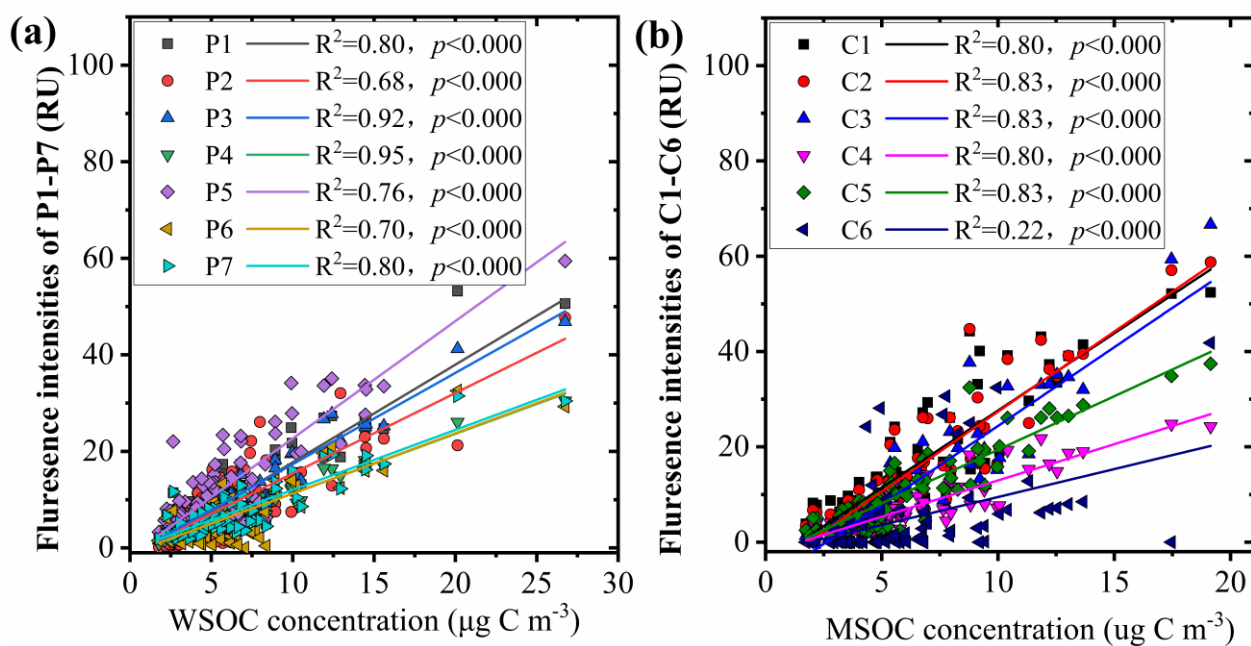


**Figure S12.** Mean light absorption of water-soluble BrC, methanol-soluble BrC, and BC (a), and relative to total light-absorption aerosol (b) in the aerosol samples from Bangkok during 2016-2017.



185

186 **Figure S13.** Scatter plots of (a) WSOC concentration ( $\mu\text{g C m}^{-3}$ ) versus fluorescence intensities of component P1–  
 187 P7 (RU) in the WSOC fraction and (b) MSOC concentration ( $\mu\text{g C m}^{-3}$ ) versus fluorescence intensities of component  
 188 C1–C6 (RU) in the MSOC fraction in aerosol samples over Bangkok.

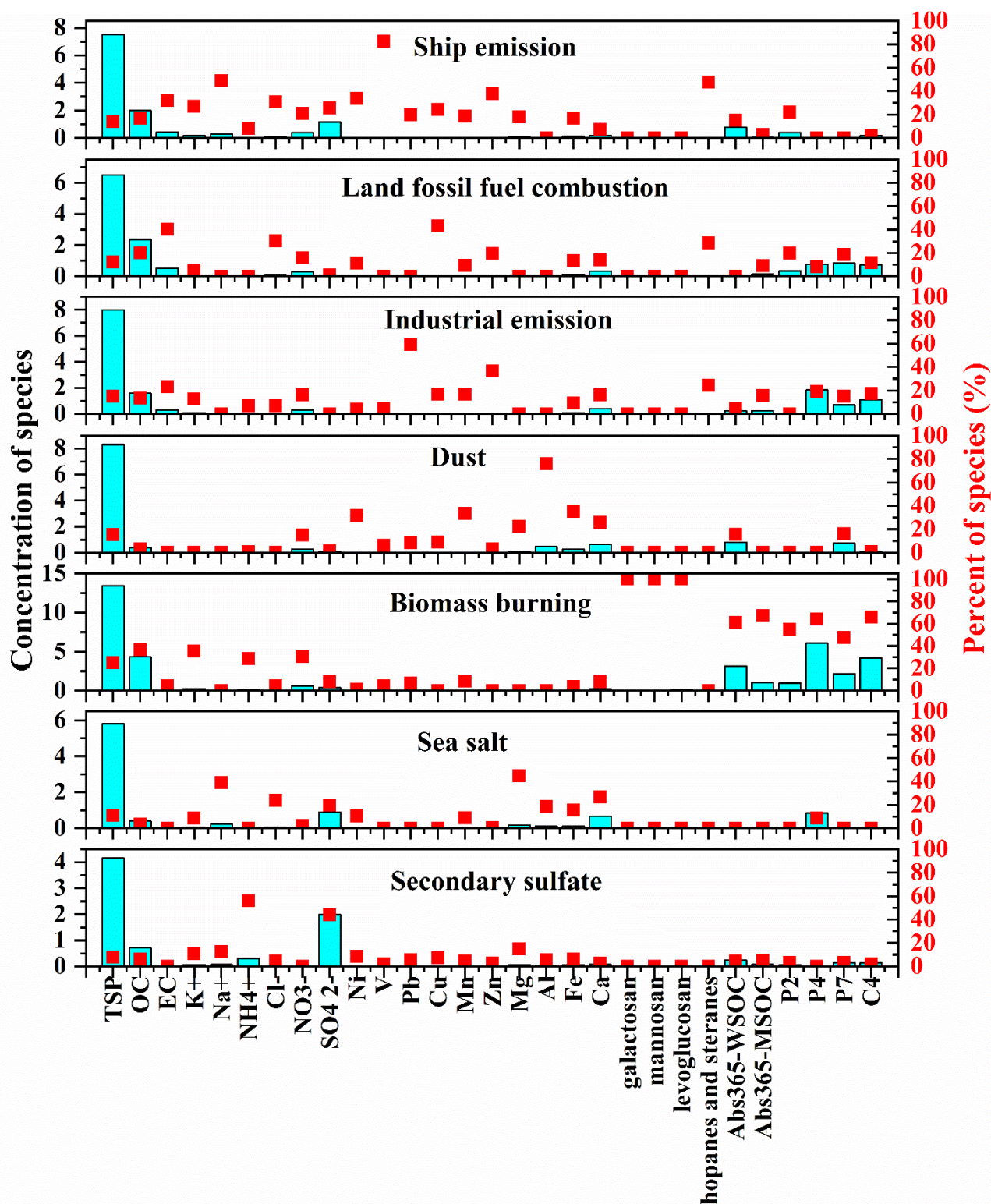


**Figure S14.** Factor profiles resolved by positive matrix factorization mode. The bars represent the concentrations of species and the dots represent the contributions of species appointed to the factors. The run method was detailly described elsewhere (Wang et al., 2020).

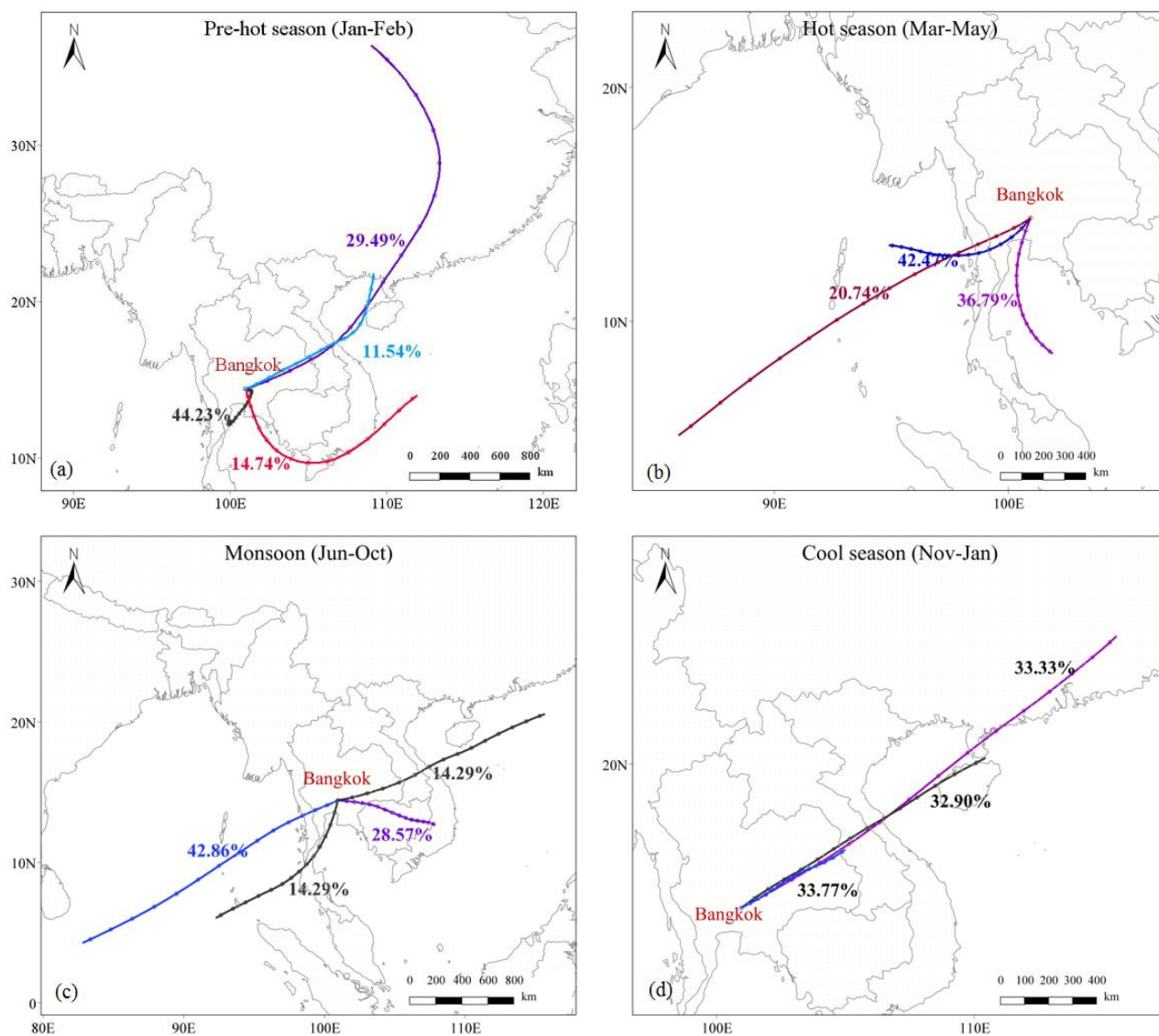


**Figure S15.** The 72 h back air-mass trajectories at Bangkok from Thailand during the (a) pre-hot season (January to February 2016), (b) hot season (March to May 2016), (c) monsoon (June to October in 2016), (d) cool season (November 2016 to January 2017). The air-mass trajectories were analyzed by HYSPLIT model.



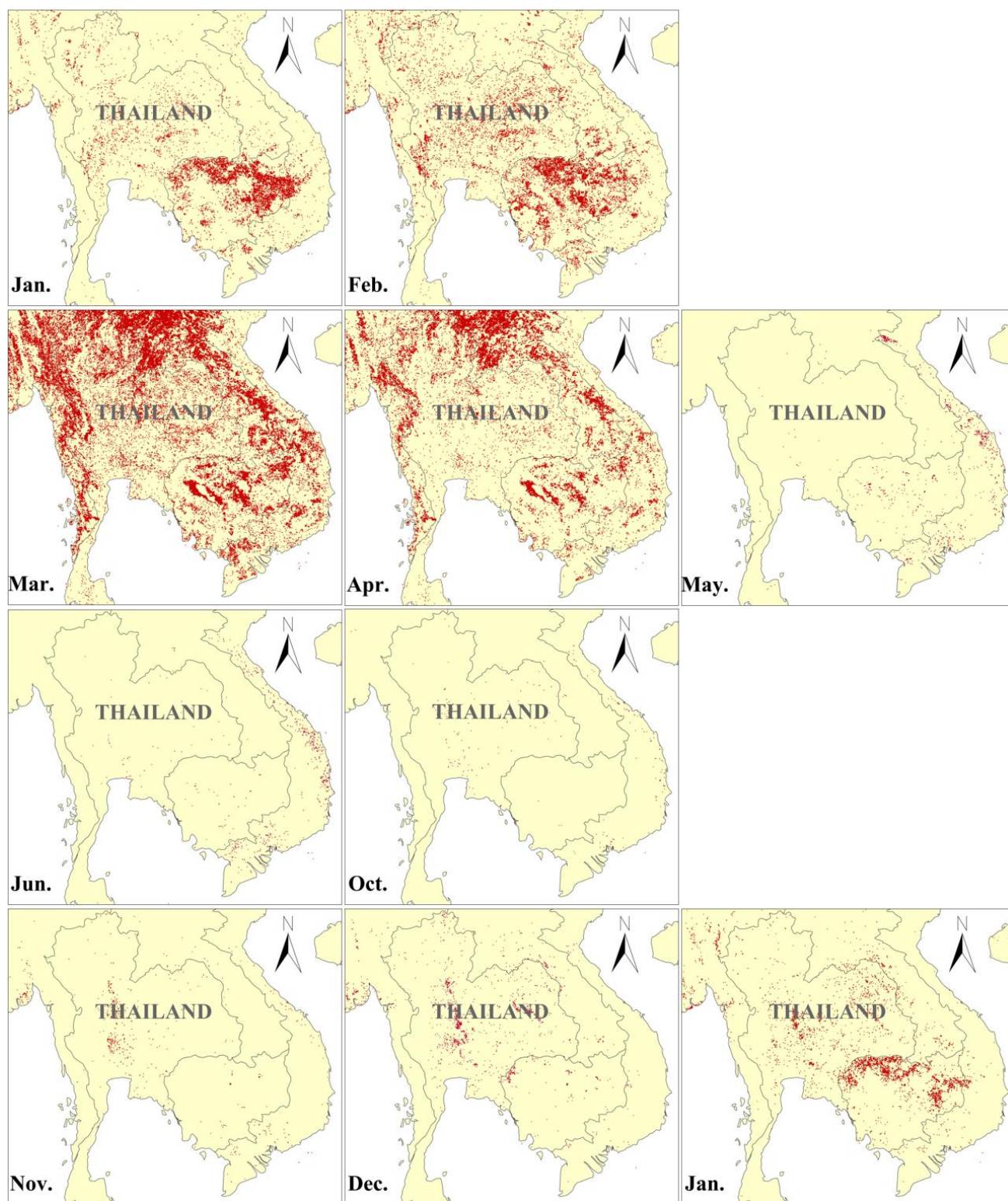


**Figure S16.** The spatial distribution of active fire spots from January 2016 to January 2017 over Thailand, which was downloaded from Moderate Resolution Imaging Spectroradiometer (MODIS) provided by NASA's Fire Information for Resource Management System (FIRMS).

#### References:

Andreae, M. O., and Gelencsér, A.: Black carbon or brown carbon? The nature of light-absorbing carbonaceous

203 aerosols, *Atmos. Chem. Phys.*, 6, 3131-3148, <https://10.5194/acp-6-3131-2006>, 2006.

204 Babar, Z. B., Park, J.-H., and Lim, H.-J.: Influence of NH<sub>3</sub> on secondary organic aerosols from the ozonolysis and  
 205 photooxidation of  $\alpha$ -pinene in a flow reactor, *Atmos. Environ.*, 164, 71-84,  
 206 <https://10.1016/j.atmosenv.2017.05.034>, 2017.

207 Barnard, J. C., Volkamer, R., and Kassianov, E. I.: Estimation of the mass absorption cross section of the organic  
 208 carbon component of aerosols in the Mexico City Metropolitan Area, *Atmos. Chem. Phys.*, 8, 6665-6679,  
 209 <http://10.5194/acp-8-6665-2008>, 2008.

210 Bond, T. C., and Bergstrom, R. W.: Light Absorption by Carbonaceous Particles: An Investigative Review, *Aerosol*  
 211 *Sci. Technol.*, 40, 27-67, <https://10.1080/02786820500421521>, 2006.

212 Chen, H., Liao, Z. L., Gu, X. Y., Xie, J. Q., Li, H. Z., and Zhang, J.: Anthropogenic Influences of Paved Runoff and  
 213 Sanitary Sewage on the Dissolved Organic Matter Quality of Wet Weather Overflows: An Excitation-Emission  
 214 Matrix Parallel Factor Analysis Assessment, *Environ. Sci. Technol.*, 51, 1157-1167,  
 215 <https://doi.org/10.1021/acs.est.6b03727>, 2017a.

216 Chen, Q., Ikemori, F., and Mochida, M.: Light Absorption and Excitation-Emission Fluorescence of Urban Organic  
 217 Aerosol Components and Their Relationship to Chemical Structure, *Environ. Sci. Technol.*, 50, 10859-10868,  
 218 <https://doi.org/10.1021/acs.est.6b02541>, 2016a.

219 Chen, Q., Miyazaki, Y., Kawamura, K., Matsumoto, K., Coburn, S., Volkamer, R., Iwamoto, Y., Kagami, S., Deng,  
 220 Y., Ogawa, S., Ramasamy, S., Kato, S., Ida, A., Kajii, Y., and Mochida, M.: Characterization of Chromophoric  
 221 Water-Soluble Organic Matter in Urban, Forest, and Marine Aerosols by HR-ToF-AMS Analysis and Excitation-  
 222 Emission Matrix Spectroscopy, *Environ. Sci. Technol.*, 50, 10351-10360,  
 223 <https://doi.org/10.1021/acs.est.6b01643>, 2016b.

224 Chen, Q., Ikemori, F., Nakamura, Y., Vodicka, P., Kawamura, K., and Mochida, M.: Structural and Light-Absorption  
 225 Characteristics of Complex Water-Insoluble Organic Mixtures in Urban Submicrometer Aerosols, *Environ. Sci.*  
 226 *Technol.*, 51, 8293-8303, <https://doi.org/10.1021/acs.est.7b01630>, 2017b.

227 Chen, Q., Mu, Z., Song, W., Wang, Y., Yang, Z., Zhang, L., and Zhang, Y. L.: Size - Resolved Characterization of the  
 228 Chromophores in Atmospheric Particulate Matter From a Typical Coal - Burning City in China, *J. Geophys.*  
 229 *Res.-Atmos.*, 124, 10546-10563, <https://10.1029/2019jd031149>, 2019.

230 Chen, W., Westerhoff, P., Leenheer, J. A., and Booksh, K.: Fluorescence excitation - Emission matrix regional  
 231 integration to quantify spectra for dissolved organic matter, *Environ. Sci. Technol.*, 37, 5701-5710,  
 232 <https://10.1021/es034354c>, 2003.

233 Chen, Y., Ge, X., Chen, H., Xie, X., Chen, Y., Wang, J., Ye, Z., Bao, M., Zhang, Y., and Chen, M.: Seasonal light  
 234 absorption properties of water-soluble brown carbon in atmospheric fine particles in Nanjing, China, *Atmos.*  
 235 *Environ.*, 230-240, <https://doi.org/10.1016/j.atmosenv.2018.06.002>, 2018.

236 Cheng, Y., He, K. B., Zheng, M., Duan, F. K., Du, Z. Y., Ma, Y. L., Tan, J. H., Yang, F. M., Liu, J. M., Zhang, X. L.,  
 237 Weber, R. J., Bergin, M. H., and Russell, A. G.: Mass absorption efficiency of elemental carbon and water-  
 238 soluble organic carbon in Beijing, China, *Atmos. Chem. Phys.*, 11, 11497-11510, [https://10.5194/acp-11-11497-](https://10.5194/acp-11-11497-2011)  
 239 [2011](https://10.5194/acp-11-11497-2011), 2011.

240 Cheng, Y., He, K.-b., Du, Z.-y., Engling, G., Liu, J.-m., Ma, Y.-l., Zheng, M., and Weber, R. J.: The characteristics of

241 brown carbon aerosol during winter in Beijing, *Atmos. Environ.*, 127, 355-364,  
 242 <https://10.1016/j.atmosenv.2015.12.035>, 2016.

243 Dasari, S., Andersson, A., Bikkina, S., Holmstrand, H., Budhavant, K., Satheesh, S. K., Asmi, E., Kesti, J., Backman,  
 244 J., and Salam, A.: Photochemical degradation affects the light absorption of water-soluble brown carbon in the  
 245 South Asian outflow, *Sci. Adv.*, 5, <https://10.1126/sciadv.aau8066>, 2019.

246 Fan, X., Wei, S., Zhu, M., Song, J., and Peng, P. a.: Comprehensive characterization of humic-like substances in  
 247 smoke PM<sub>2.5</sub> emitted from the combustion of biomass materials and fossil fuels, *Atmos. Chem. Phys.*, 16,  
 248 13321-13340, <https://doi.org/10.5194/acp-16-13321-2016>, 2016.

249 Fan, X., Li, M., Cao, T., Cheng, C., Li, F., Xie, Y., Wei, S., Song, J., and Peng, P. a.: Optical properties and oxidative  
 250 potential of water- and alkaline-soluble brown carbon in smoke particles emitted from laboratory simulated  
 251 biomass burning, *Atmos. Environ.*, 194, 48-57, <https://10.1016/j.atmosenv.2018.09.025>, 2018.

252 Gao, Y., and Zhang, Y.: Formation and photochemical investigation of brown carbon by hydroxyacetone reactions  
 253 with glycine and ammonium sulfate, *RSC Advances*, 8, 20719-20725, <https://10.1039/c8ra02019a>, 2018.

254 Hoffer, A., Gelencsér, A., Guyon, P., Kiss, G., Schmid, O., Frank, G., Artaxo, P., and Andreae, M.: Optical properties  
 255 of humic-like substances (HULIS) in biomass-burning aerosols, *Atmos. Chem. Phys.*, 6, 3563-3570,  
 256 <https://10.5194/acp-6-3563-2006>, 2006.

257 Lee, H. J., Aiona, P. K., Laskin, A., Laskin, J., and Nizkorodov, S. A.: Effect of solar radiation on the optical properties  
 258 and molecular composition of laboratory proxies of atmospheric brown carbon, *Environ. Sci. Technol.*, 48,  
 259 10217-10226, <https://10.1021/es502515r>, 2014.

260 Liu, C., Chung, C. E., Yin, Y., and Schnaiter, M.: The absorption Ångström exponent of black carbon: from numerical  
 261 aspects, *Atmos. Chem. Phys.*, 18, 6259-6273, <https://10.5194/acp-18-6259-2018>, 2018a.

262 Liu, J., Bergin, M., Guo, H., King, L., Kotra, N., Edgerton, E., and Weber, R. J.: Size-resolved measurements of  
 263 brown carbon in water and methanol extracts and estimates of their contribution to ambient fine-particle light  
 264 absorption, *Atmos. Chem. Phys.*, 13, 12389-12404, <https://10.5194/acp-13-12389-2013>, 2013.

265 Liu, J., Mo, Y., Ding, P., Li, J., Shen, C., and Zhang, G.: Dual carbon isotopes (<sup>14</sup>C and <sup>13</sup>C) and optical properties of  
 266 WSOC and HULIS-C during winter in Guangzhou, China, *Sci. Total Environ.*, 633, 1571-1578,  
 267 <https://doi.org/10.1016/j.scitotenv.2018.03.293>, 2018b.

268 Mo, Y., Li, J., Jiang, B., Su, T., Geng, X., Liu, J., Jiang, H., Shen, C., Ding, P., Zhong, G., Cheng, Z., Liao, Y., Tian,  
 269 C., Chen, Y., and Zhang, G.: Sources, compositions, and optical properties of humic-like substances in Beijing  
 270 during the 2014 APEC summit: Results from dual carbon isotope and Fourier-transform ion cyclotron resonance  
 271 mass spectrometry analyses, *Environ. Pollut.*, 239, 322-331, <https://doi.org/10.1016/j.envpol.2018.04.041>, 2018.

272 Murphy, K. R., Stedmon, C. A., Wenig, P., and Bro, R.: OpenFluor– an online spectral library of auto-fluorescence  
 273 by organic compounds in the environment, *Anal. Methods*, 6, 658-661, <https://10.1039/c3ay41935e>, 2014.

274 Park, S. S., and Yu, J.: Chemical and light absorption properties of humic-like substances from biomass burning  
 275 emissions under controlled combustion experiments, *Atmos. Environ.*, 136, 114-122,  
 276 <https://doi.org/10.1016/j.atmosenv.2016.04.022>, 2016.

277 Pohlker, C., Huffman, J. A., and Pöschl, U.: Autofluorescence of atmospheric bioaerosols – fluorescent biomolecules  
 278 and potential interferences, *Atmos. Meas. Tech.*, 5, 37-71, <https://10.5194/amt-5-37-2012>, 2012.

279 Qin, J., Zhang, L., Zhou, X., Duan, J., Mu, S., Xiao, K., Hu, J., and Tan, J.: Fluorescence fingerprinting properties  
 280 for exploring water-soluble organic compounds in PM<sub>2.5</sub> in an industrial city of northwest China, *Atmos.*  
 281 *Environ.*, 184, 203-211, <https://doi.org/10.1016/j.atmosenv.2018.04.049>, 2018.

282 Shetty, N. J., Pandey, A., Baker, S., Hao, W. M., and Chakrabarty, R. K.: Measuring light absorption by freshly emitted  
 283 organic aerosols: optical artifacts in traditional solvent-extraction-based methods, *Atmos. Chem. Phys.*, 19,  
 284 8817-8830, <https://10.5194/acp-19-8817-2019>, 2019.

285 Stedmon, C. A., and Markager, S.: Resolving the variability in dissolved organic matter fluorescence in a temperate  
 286 estuary and its catchment using PARAFAC analysis, *Limnol. Oceanogr.*, 50, 686-697,  
 287 <https://10.4319/lo.2005.50.2.0686>, 2005.

288 Tang, J., Li, J., Mo, Y., Safaei Khorram, M., Chen, Y., Tang, J., Zhang, Y., Song, J., and Zhang, G.: Light absorption  
 289 and emissions inventory of humic-like substances from simulated rainforest biomass burning in Southeast Asia,  
 290 *Environ. Pollut.*, 262, 114266, <https://doi.org/10.1016/j.envpol.2020.114266>, 2020a.

291 Tang, J., Li, J., Su, T., Han, Y., Mo, Y., Jiang, H., Cui, M., Jiang, B., Chen, Y., Tang, J., Song, J., Peng, P., and Zhang,  
 292 G.: Molecular compositions and optical properties of dissolved brown carbon in biomass burning, coal  
 293 combustion, and vehicle emission aerosols illuminated by excitation–emission matrix spectroscopy and Fourier  
 294 transform ion cyclotron resonance mass spectrometry analysis, *Atmos. Chem. Phys.*, 20, 2513-2532,  
 295 <https://10.5194/acp-20-2513-2020>, 2020b.

296 Wang, J., Jiang, H., Jiang, H., Mo, Y., Geng, X., Li, J., Mao, S., Bualert, S., Ma, S., Li, J., and Zhang, G.: Source  
 297 apportionment of water-soluble oxidative potential in ambient total suspended particulate from Bangkok:  
 298 Biomass burning versus fossil fuel combustion, *Atmos. Environ.*, 235, 117624,  
 299 <https://doi.org/10.1016/j.atmosenv.2020.117624>, 2020.

300 Wu, G., Ram, K., Fu, P., Wang, W., Zhang, Y., Liu, X., Stone, E. A., Pradhan, B. B., Dangol, P. M., Panday, A. K.,  
 301 Wan, X., Bai, Z., Kang, S., Zhang, Q., and Cong, Z.: Water-Soluble Brown Carbon in Atmospheric Aerosols  
 302 from Godavari (Nepal), a Regional Representative of South Asia, *Environ. Sci. Technol.*, 53, 3471-3479,  
 303 <https://doi.org/10.1021/acs.est.9b00596>, 2019.

304 Wünsch, U. J., Bro, R., Stedmon, C. A., Wenig, P., and Murphy, K. R.: Emerging patterns in the global distribution  
 305 of dissolved organic matter fluorescence, *Anal. Methods*, 11, 888-893, <https://10.1039/c8ay02422g>, 2019.

306 Xie, C., Xu, W., Wang, J., Wang, Q., Liu, D., Tang, G., Chen, P., Du, W., Zhao, J., Zhang, Y., Zhou, W., Han, T., Bian,  
 307 Q., Li, J., Fu, P., Wang, Z., Ge, X., Allan, J., Coe, H., and Sun, Y.: Vertical characterization of aerosol optical  
 308 properties and brown carbon in winter in urban Beijing, China, *Atmos. Chem. Phys.*, 19, 165-179,  
 309 <https://10.5194/acp-19-165-2019>, 2019a.

310 Xie, M., Chen, X., Holder, A. L., Hays, M. D., Lewandowski, M., Offenberg, J. H., Kleindienst, T. E., Jaoui, M., and  
 311 Hannigan, M. P.: Light absorption of organic carbon and its sources at a southeastern U.S. location in summer,  
 312 *Environ. Pollut.*, 244, 38-46, <https://10.1016/j.envpol.2018.09.125>, 2019b.

313 Yan, C., Zheng, M., Sullivan, A. P., Bosch, C., Desyaterik, Y., Andersson, A., Li, X., Guo, X., Zhou, T., Gustafsson,  
 314 Ö., and Collett, J. L.: Chemical characteristics and light-absorbing property of water-soluble organic carbon in  
 315 Beijing: Biomass burning contributions, *Atmos. Environ.*, 121, 4-12,  
 316 <https://doi.org/10.1016/j.atmosenv.2015.05.005>, 2015.



317 Zhou, Y., Wen, H., Liu, J., Pu, W., Chen, Q., and Wang, X.: The optical characteristics and sources of chromophoric  
318 dissolved organic matter (CDOM) in seasonal snow of northwestern China, *The Cryosphere*, 13, 157-175,  
319 <https://10.5194/tc-13-157-2019>, 2019.